ARMY RESEARCH LABORATORY

Boundary Layer Turbulence (BLT) Water Vapor Measurement Test: Summary of Current Results September 2009

by Sean O'Brien, David Tofsted, Jimmy Yarbrough, D. Scott Elliott, David Quintis, and Robert Brice

ARL-TR-4991 **October 2009**

NOTICES

Disclaimers

The findings in this report are not to be construed as an official Department of the Army position unless so designated by other authorized documents.

Citation of manufacturer's or trade names does not constitute an official endorsement or approval of the use thereof.

Destroy this report when it is no longer needed. Do not return it to the originator.

Army Research Laboratory
White Sands Missile Range, NM 88002-5513

ARL-TR-4991 **October 2009**

Boundary Layer Turbulence (BLT) Water Vapor Measurement Test: Summary of Current Results September 2009

Sean O'Brien, David Tofsted, Jimmy Yarbrough,
D. Scott Elliott, David Quintis, and Robert Brice
Computational Information Sciences Directorate, ARL

REPORT DOCUMENTATION PAGE	Form Approved OMB No. 0704-0188

1. REPORT DATE *(DD-MM-YYYY)*	2. REPORT TYPE	3. DATES COVERED (From - To)
October 2009	Final	May 2007–October 2007

4. TITLE AND SUBTITLE
Boundary Layer Turbulence (BLT) Water Vapor Measurement Test: Summary of Current Results September 2009

5a. CONTRACT NUMBER

5b. GRANT NUMBER

5c. PROGRAM ELEMENT NUMBER

6. AUTHOR(S)
Sean O'Brien, David Tofsted, Jimmy Yarbrough, D. Scott Elliott, David Quintis, and Robert Brice

5d. PROJECT NUMBER

5e. TASK NUMBER

5f. WORK UNIT NUMBER

7. PERFORMING ORGANIZATION NAME(S) AND ADDRESS(ES)
U.S. Army Research Laboratory
Computational and Information Sciences Directorate
Battlefield Environment Division (ATTN: RDRL-CIE-D)
White Sands Missile Range, NM 88002-5501

8. PERFORMING ORGANIZATION REPORT NUMBER
ARL-TR-4991

9. SPONSORING/MONITORING AGENCY NAME(S) AND ADDRESS(ES)
U.S. Army Research Laboratory
2800 Powder Mill Road
Adelphi, MD 20783-1145

10. SPONSOR/MONITOR'S ACRONYM(S)

11. SPONSOR/MONITOR'S REPORT NUMBER(S)

12. DISTRIBUTION/AVAILABILITY STATEMENT
Approved for public release; distribution is unlimited.

13. SUPPLEMENTARY NOTES

14. ABSTRACT
The propagation of terahertz (THz) band radiation through the atmosphere is a topic of increasing interest as advanced passive and active imaging systems are developed that operate in this spectral region. Much of the impact of the boundary layer atmosphere in this band is due to water vapor absorption, which is very strong even in atmospheric window regions. Most of the effect of atmospheric water vapor is due to the average integrated path value. However, absorption effects are so extreme in the THz band that short-path variability of water vapor can play a mitigating role. To study this variability in the boundary layer we performed a field measurement experiment. The purpose of this experiment was to measure atmospheric water vapor temporal and spatial structure with the highest practical resolution. We describe the setup of the test sensors, data collection procedures, and analysis results below.

15. SUBJECT TERMS
turbulence, stability, surface layer, characterization, terahertz, water vapor

16. SECURITY CLASSIFICATION OF:			17. LIMITATION OF ABSTRACT	18. NUMBER OF PAGES	19a. NAME OF RESPONSIBLE PERSON
a. REPORT	b. ABSTRACT	c. THIS PAGE			Sean O'Brien
Unclassified	Unclassified	Unclassified	UU	38	19b. TELEPHONE NUMBER (*Include area code*) (575) 678-1570

Standard Form 298 (Rev. 8/98)
Prescribed by ANSI Std. Z39.18

Contents

List of Figures

List of Tables

Preface

The Boundary Layer Turbulence (BLT) test was designed as part of a larger effort to characterize the propagation properties of the near-surface atmosphere for simulation and prediction of terahertz frequency band system performance. The principal limiting factor for system performance in field operation is the strong absorption of terahertz energy by atmospheric water vapor. Earlier studies using scanned Light Detection and Ranging (LIDAR) probes indicated that significant turbulent water vapor density structure exists in the boundary layer. This turbulent structure will modulate the spatial frequency composition of terahertz band imagery and will also temporally modulate terahertz band communication links. As a first step toward a truly comprehensive treatment, it was decided to characterize the boundary layer water vapor turbulence for the desert environment with an instrument suite consisting of high speed hygrometers and anemometers.

The results of this field experiment were first used to refine the spatial frequency spectrum model used by a terahertz image propagation model that we had developed as part of our contribution to the Defense Advanced Research Projects Agency (DARPA)-sponsored Terahertz Imaging Focal-plane-array Technology (TIFT) project. However, many other applications for the BLT data and their analytical products are possible. For example, high energy laser systems operating at wavelengths where water vapor is a significant absorber can experience significant blooming behavior within regions where the absolute humidity is stochastically high. Another application for the BLT data is in the assessment of short range covert terahertz communication links that may be intermittently visible at longer ranges due to spatial fluctuations in the water vapor density field.

The report that follows is our initial documentation that describes the test design, physical layout, configuration sequence, and preliminary analytical results. We intend to build on this effort with future analytical reports that will examine the data in greater detail.

Acknowledgments

The authors wish to thank Dr. Mark Rosker of DARPA for his support of our modeling effort under the TIFT program. We also wish to thank other TIFT team members for their support of our effort, including Dr. Eddie Jacobs of U.S. Army Night Vision and Electronic Sensors Directorate (NVESD) (now with the University of Memphis), Mr. Richard Espinola of NVESD, Dr. Stephen Griffin of the University of Memphis, Dr. Frank De Lucia of Ohio State University, and Mr. Douglas Petkie of Wright State University.

Executive Summary

The Battlefield Environment Division, part of the U.S. Army Research Laboratory's (ARL) Computational and Information Science Directorate, has worked extensively in boundary layer meteorology to further the Army's knowledge of atmospheric influences on various types of battlefield sensing technologies. Two such emergent technologies are imaging sensors operating in the terahertz (THz) band of the electromagnetic spectrum, and short-haul THz-based communications systems. Water vapor absorption in this band is significant in the boundary layer. Even the best THz window regions feature absorption coefficients near 0.1 dB/m for mid-range values of absolute humidity. Consequently, the effective range of THz active sensor illumination may vary greatly, depending on the nature of the ambient atmosphere under different propagation conditions, since the amount of water vapor present in the atmosphere is a strong function of terrain and weather.

There is considerable uncertainty regarding the overall degree of variation possible in the path integrated moisture, which is dependent on fluctuations in atmospheric humidity levels due to turbulent influences.[1] Although some knowledge of these fluctuations is available, based on studies of "conservative passive additive" scalar fluctuation effects featured in dynamic similarity theory, humidity influences must be treated somewhat differently from temperature influences. In particular, temperature fluctuations are derived from heat transfers at the surface using a similar mechanism for all surfaces, whereas humidity sources can arise from spatially localized vegetative or surface water features, and can have more complex emission rate scenarios.

We designed the Boundary Layer Turbulence (BLT) experiment[2] to provide a database of simultaneous wind, temperature, and absolute humidity turbulence measurements by multiple sensor platforms at high temporal and spatial resolution over an extended period of weeks. The experiment proceeded in phases, from an initial intercomparison of sensors, to a series of horizontal (single level) array configurations, to a two-dimensional triangular pattern, and finally to vertical tower-horizontal array combination. As we proceeded, we applied "lessons learned" to our data acquisition and reduction procedures to fix problems due to instrumental and environmental phenomena.

The BLT experiment was conducted during the late spring (from mid-May) and summer (to early August) seasons at our White Sands Missile Range (WSMR), NM, observation site. The

[1] O'Brien, S. G.; Tofsted, D. H. Terahertz Target Fluctuation Estimates Derived from Field Measurements of Atmospheric Water Vapor. *Proceeding of the SPIE Defense and Security Conference,* Vol. 6949, Orlando, FL, 2008.

[2] O'Brien, S. G.; Tofsted, D. H.; Yarbrough, J.; Scott Elliott, D.; Quintis, D. Analysis of Boundary Layer Meteorological Data Collected at the White Sands Missile Range. *Proceeding of the SPIE Defense and Security Conference,* Vol. 6239, Orlando, FL, 2006., Las Cruces, NM, December 2007.

precipitation patterns that occurred during the experimental period deviated from the expected climatological norms. The main departure from the climatology was in late May 2007, where the frequency of thunderstorm activity was higher than usual. This pattern persisted into the normally quiet early June period that precedes the more active late June to early September monsoonal season at WSMR. As a result, we observed unusually high latent heat fluxes in our early results and also observed heavy rain conditions that caused our fast hygrometer sensors to produce intermittently erroneous measurements.

The primary analysis products that we generated to understand the results of our experiment are spatial frequency spectra for the absolute humidity turbulence, inner and outer size scales for this turbulence, and correlation of latent heat flux behavior with local weather conditions. Secondary products include spectral and flux correlations for wind speed, wind direction, and temperature with local weather conditions and shortwave/longwave radiative fluxes.

The database that we have developed should provide valuable insight into the effect of the atmosphere (particularly the desert boundary layer) upon THz imaging and communication systems. In parallel, we have developed an imaging tool[3] that may be used to simulate the effects of a turbulent environment upon the image quality observed by prospective passive and active THz imagers. In our initial investigations, we have seen many interesting daytime and nocturnal boundary layer phenomena; we expect that more will be uncovered as we perform additional detailed spectral, cross correlation, and covariance analyses. Data auditing software has been developed to uncover problems with instruments and atmospheric conditions that might complicate or invalidate results from analysis software during the data reduction process. We will continue to refine our reduction and analysis software to capture the temporal and spatial scales that can be observed for humidity fluctuations, and compare these with what might be expected from theory.

[3] O'Brien, S. G.; Tofsted, D. Development of a Terahertz Short Range Imaging Model. *Proceeding of the SPIE Defense and Security Conference*, Vol. 6239, Orlando, FL, 2006.

1. Introduction

The Battlefield Environment Division of the U.S. Army Research Laboratory (ARL) has worked extensively in boundary layer meteorology to further the Army's knowledge of atmospheric influences on various types of battlefield sensing technologies. One of these emerging technologies is imaging sensors operating in the terahertz (THz) band of the electromagnetic spectrum. This band features radiation wavelengths of approximately ½ mm (500 microns) or less. Of particular interest is propagation in the band around 650 GHz, a so-called atmospheric window region, yet even this band features significant water vapor absorption.

To be more specific, the absorption in this waveband is approximately 0.1 dB/m for mid-range absolute humidity levels, which yields effective ranges for imaging equipment of 50–200 m. However, the degree of the variation in this effective range may greatly depend on the nature of the ambient atmosphere under different propagation conditions, since the amount of water vapor present in the atmosphere is a strong function of terrain and weather conditions.

There is also considerable uncertainty regarding the overall degree of variation possible in the path-integrated moisture that depends on fluctuations in atmospheric humidity levels due to turbulent influences. Although some knowledge of these fluctuations is available, based on studies of "conservative passive additive" scalar fluctuation effects featured in dynamic similarity theory, humidity influences must be treated somewhat differently from temperature influences. In particular, temperature fluctuations are derived from the sensible heat flux at various surfaces (e.g., Oke, 1978), whereas humidity sources can arise from spatially localized vegetative or surface water features, and can have more complex emission rate scenarios. One such feature is the plant stomatal resistance that depends on the ambient humidity level and available soil moisture (e.g., Deardorff, 1977). The diversity of water vapor sources raises several questions that are relevant to the structure of humidity fluctuations. For instance, are there feasible methods (such as air mass trajectory analysis) to determine source points of an observed water vapor field? What is the mechanism that creates humidity fluctuations from standing pools of water, grass, shrubbery, and trees as they are ventilated by ambient winds? Can these sources somehow be characterized by identifiable signatures? What are the influences of anthropogenic artifacts such as buildings and landscaping on water source emissions? Must such effects be treated on an individualized basis or is it possible to aggregate the results into more general models?

Most studies of water effects are motivated mainly by agricultural concerns. As a result, much of the available information is based on evaporation of water from roughly uniform crop surfaces. In contrast, our interest is primarily in urban or other short-range settings that may feature individualized (non-uniform) water sources. We are interested in both horizontal and vertical fluctuations, since particularly at night there may be a highly concentrated moist layer

near the ground due to the suppression of vertical mixing. We are also interested in the spatial spectral nature of these fluctuations since fluctuations at different size scales will have different influences on the propagation problem. For instance, large fluctuations at small scales may be significant, leading to image degradation, whereas large scale fluctuations may not be significant at all, since they merely contribute to the overall extinction along a path.

With these considerations in mind, we proposed, designed, and executed the Boundary Layer Turbulence (BLT) experiment (O'Brien et al., 2007) to provide a body of information that can be used to examine the impact of boundary layer water vapor turbulence upon THz systems.

2. Background and Review of Test Methodology

2.1 Summary of Prior Results and Motivation for the Current Work

Our initial high speed water vapor fluctuation measurements were collected in March (near Building 19472 at White Sands Missile Range [WSMR], NM) and August 2005 (at a suburban site in Las Cruces, NM), using a single Li-Cor transmissometer sensor flanked by multiple UVW ultrasonic anemometers (R. M. Young model 81000). Because only one Li-Cor humidity probe was available for these earlier measurements, analysis was limited to stream-wise fluctuations at a fixed spatial point. The spectra that were derived from these data were used to create three-dimensional (3D) synthetic stochastic humidity fields in a THz image propagation model that was developed in collaboration with the Defense Advanced research Projects Agency (DARPA)-sponsored THz Imaging Focal-plane-array Technology (TIFT) project.

Since those initial measurements, two additional Li-Cor probes were purchased for the BLT measurement effort. Consequently, we can now answer a wider range of characterization questions than was previously possible. In particular, we can now obtain simultaneous data at three points with variable spatial separations, so correlation analysis of these data can produce valuable insights into the nature of the water vapor fluctuation spectra in both vertical and horizontal planes. Additionally, we can, as before, deduce correlations between the humidity fluctuations and other meteorological data such as wind speed and direction that are collected simultaneously. We developed the measurement program described below to at least partially address the following questions:

- How do the humidity spectrum inner and outer scales vary as a function of height?
- What is the vertical structure of humidity fluctuations, and how does it vary with time of day?
- How does the vertical flux of latent heat vary with time of day and prevailing wind direction?

- How well can we determine outer scale for the humidity fluctuations in the vertical and horizontal by varying sensor separation and cross-correlating the sensor data?
- Can we correlate long and short range airmass trajectories over terrain and vegetation features with the mean value of humidity and the strength of humidity fluctuations?
- How good is the Taylor's "frozen field" hypothesis for humidity fluctuations?
- Can we see gravity wave or drainage flow effects in the humidity mean or fluctuation data?

The information provided by these inquiries will improve the accuracy of THz image propagation and sensor performance models, particularly in situations where the sensor system has a large field of view or field of regard.

2.2 Geographical Description of the Test Site

The test site was chosen on the basis of convenience and security for the ARL staff who conducted and maintained the experiment. The measurement instruments were sited next to the Building 19472 compound, outside of the fence perimeter and placed up-wind from the fence by approximately 20 m to avoid influences of the fence on the measurements obtained. The terrain at the test site is nearly flat, but slightly slopes downhill toward the northeast. Spurs of the Organ Mountains are nearby to the west and southwest of the test site. Figures 1, 2, and 3 are satellite images of the terrain near the test site extracted from the Internet with some contrast enhancement to reduce atmospheric haze. These are presented in order of increasing detail, with the last image depicting the approximate location of the horizontal measurement array.

Figure 1. Wide field satellite image of the Bldg. 19472 test site and its environs, which are located at the terminus of a road spur. Note the light-colored dry wash at lower left of picture. North is the vertical upward direction.

Figure 2. Higher spatial resolution image of test site. Note that the larger patches of vegetation are primarily mesquite, with smaller patches consisting of mesquite, creosote bush, and yucca. The largest plants are of the order of 2 m tall.

Figure 3. At the highest resolution, the compound perimeter fence is clearly seen, along with the approximate location of the horizontal measurement array (which is indicated by the red dot).

The area is sparsely vegetated with plants that are typical of the Chihuahuan desert environment: mesquite, creosote bush, and various species of yucca. There are also smaller plants and grasses present on the test site terrain whose density varies greatly with the amount of recent rainfall during the growing season. The rainfall (mostly in the form of thunder showers) was noticeably greater than usual during the early part of the test period, resulting in enhanced small plant coverage and growth.

The soil at the test site is primarily sand, with some amendment of organic matter from plant decay. Small mammals, reptiles, insects, and other animals recycle this plant material through various levels of the food chain. As an indirect result, much of the soil is well aerated and is

permeated by burrows, scrapes, and mounds. Much of the soil is so well-aerated that it is very soft; requiring much care in setting up and securing instrument tripods and towers.

2.3 Climatological Description of Test Site Region

We wished to conduct our measurement series over an extended period during which moisture levels were expected to range from very dry to fairly moist (relative to the norms for the U.S. desert Southwest). The dry period was expected to range from the beginning of the experiment in mid May through the end of June, with monsoonal enhancement of the moisture levels beginning in mid July. Surface temperatures for this period are also quite warm, with highs ranging between 85 and 100 °F and lows generally between 60 and 70 °F. Most of the rains that occur during this period are associated with thunderstorms. These are typically localized in nature, causing irregular patterns of wind speed and direction. Typical thundershower activity involves late morning cloud building and mid-afternoon to evening thundershower activity. Tables 1–5 show climatological means associated with the WSMR C-Station meteorological site, approximately 5 miles from our site.

Table 1. C-Station climatological means for air temperature (°F).

	May	Jun	Jul	Aug	Sep	Oct	Nov
Low	55	62	66	65	58	46	34
High	87	96	96	93	87	78	66
Mean	71	79	81	79	73	62	50

Table 2. C-Station climatological means for wind speed and direction.

	May	Jun	Jul	Aug	Sep	Oct	Nov
Spd (kts)	6.0	5.0	4.6	3.9	3.6	3.8	4.3
Dir	W	S	S	S	S	S	S

Table 3. C-Station climatological means for relative humidity at 0500 and 1700 local.

	May	Jun	Jul	Aug	Sep	Oct	Nov
0500	45%	50%	65%	74%	71%	65%	62%
1700	17%	19%	31%	35%	34%	31%	34%

Table 4. C-Station climatological means for precipitation.

	May	Jun	Jul	Aug	Sep	Oct	Nov
Amt (in)	0.56	0.99	1.43	2.54	1.75	0.88	0.55
Pct of Yr	5%	8%	12%	22%	15%	7%	5%

Table 5. C-Station climatological means for percentage daytime and 24-hour (h) sky cover.

	May	Jun	Jul	Aug	Sep	Oct	Nov
Day	41%	37%	52%	55%	42%	43%	40%
24 h	35%	37%	51%	55%	41%	33%	34%

Our actual experience as the late spring to summer seasons unfolded was a pronounced departure of precipitation amounts from the climatological averages. Significant thunderstorm activity began in May and continued throughout the remainder of the test period, with some multi-day respites of dry weather interspersed. Tables 6–8 list the temperature, wind, and precipitation averages observed for May–July 2007, with the associated climatological averages shown for comparison.

Table 6. C-Station 2007 observed means and extremes for air temperature (°F). C-Station climatological values are shown in parentheses.

	May	Jun	Jul
Extreme Low	43 (55)	54 (62)	62 (66)
Extreme High	93 (87)	105 (96)	101 (96)
Mean	70 (71)	81 (79)	80 (81)

Table 7. C-Station 2007 observed means and extremes for wind speed and direction. C-Station climatological values are shown in parentheses.

	May	Jun	Jul
Speed (kts)	6.1 (6.0)	6.1 (5.0)	5.2 (4.6)
Direction	208° SW (W)	274° W (S)	135° SE (S)

Table 8. C-Station 2007 observed means and extremes for precipitation. C-Station climatological values are shown in parentheses.

	May	Jun	Jul
Total (in)	1.38 (0.56)	0.76 (0.99)	2.36 (1.43)

2.4 Test Setup and Schedule

We arranged our test series in phases to make the most of the available instrumentation and to allow our personnel time to streamline experimental procedures. Roughly, these phases were organized into three episodes: pre-test (Phase 0) calibrations and shakedown tests of sensors; horizontal array measurements (Phases 1A and 1B) and combined horizontal array and vertical tower (Phases 2A and 2B) measurements. The analysis results provided in this report will primarily deal with the horizontal array measurement series, so that we shall only describe the Phase 1 and 2 setup geometry. Figures 4–7 depict the test layout for Phases 1A, 1B, 2A, and 2B respectively.

2.4.1 Phase 1A (25 May 2007 to 29 Jun 2007)

This phase of the experiment was the initial operational period, though some hardware and software configuration refinements continued to be set in place. Only the horizontal array was used for this phase, with the south-to-north line of the array oriented 330° from north. The three Li-Cor and sonic anemometer sensor pairs were separated by 2 m and were mounted at a height of 2 m on tripods. Each Li-Cor and sonic pair were separated by a horizontal distance of 20 cm, with the sonic upwind (for our initial prevailing wind direction estimate of 240° from north) from the Li-Cor.

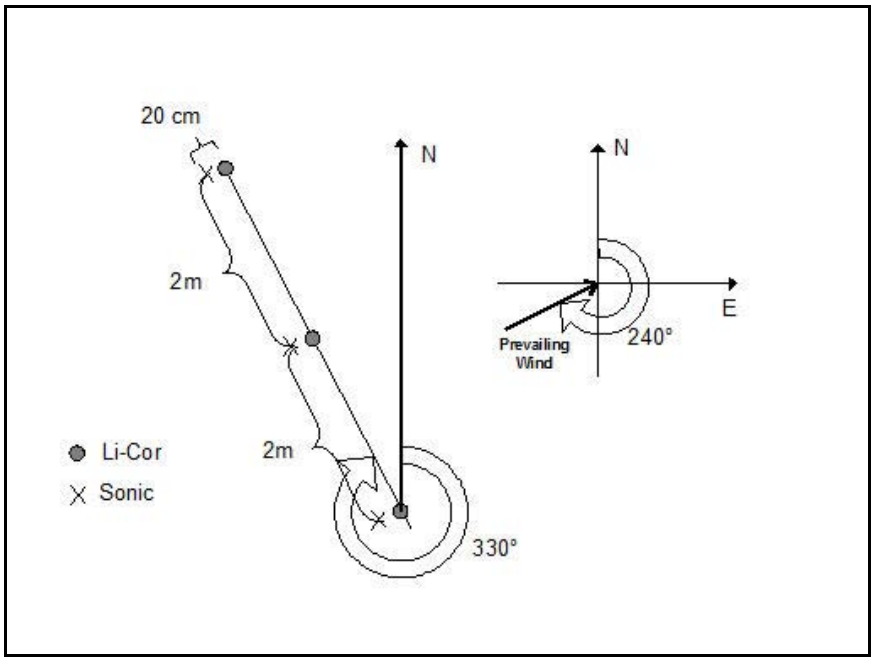

Figure 4. Phase 1A test layout for horizontal array of Li-Cor and sonic sensors.

2.4.2 Phase 1B (29 Jun 2007 to 25 Jul 2007)

The measurements collected during Phase 1A indicated that the prevailing wind was more northwesterly than our initial estimate for the observing period. We therefore took the opportunity to reorient the array line to a bearing of 20° from north as we increased the array spacing to 4 m between sensor pairs.

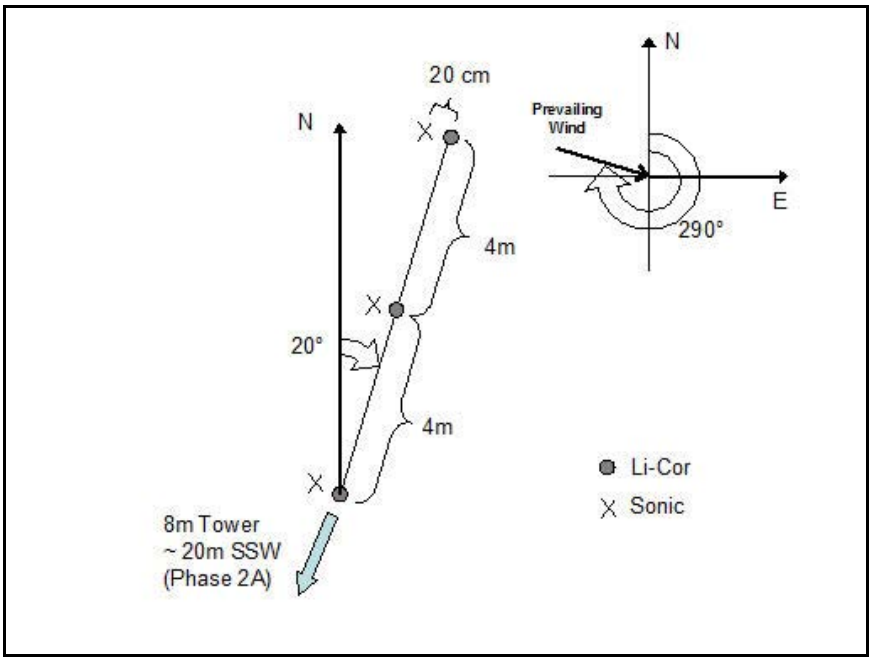

Figure 5. Phase 1B test layout for horizontal array (also used in Phase 2A).

2.4.3 Phase 2A (25 Jul 2007 to 15 Aug 2007)

This phase marked the initial operation of the 8 m vertical tower array of T107 thermistor temperature sensors and sonic anemometers, as well as the Kipp and Zonen Model CNR1 radiometric sensor set. The tower was populated at 2, 4, 6, and 8 m above ground level (AGL) with pairs of sonic and T107 sensors. This combination was selected to provide a vertical profile of temperature and wind fluctuations, with the T107s providing a more accurate estimate of the long-term mean temperature at each level. Additional T107 sensors were situated within 2 m of the tower at 1 m and 0.15 m (about 6 inches) AGL. Prior to the start of the BLT test, the T107 sensors were intercompared and calibrated by placing them in close proximity at the same (2 m AGL) height. The tower was set up to be in line with the horizontal array line, at a distance of approximately 20 m from the south end of the horizontal array line. The CNR1 sensor set was situated about 4 m from the base of the tower, at a height of 2 m, on a line between the tower and the horizontal array. The horizontal array configuration was unchanged from Phase 1B for this phase of the experiment. A photograph of this setup is shown in figure 8.

2.4.4 Phase 2B (15 Aug 2007 to 30 Sep 2007)

The horizontal array central sensor pair was moved 2 m to the south along the existing array line for this phase, to create an asymmetric 2 m, 6 m pair spacing. This was an effort to see if more simultaneous scale information could be obtained more efficiently. The tower configuration was unchanged for this phase.

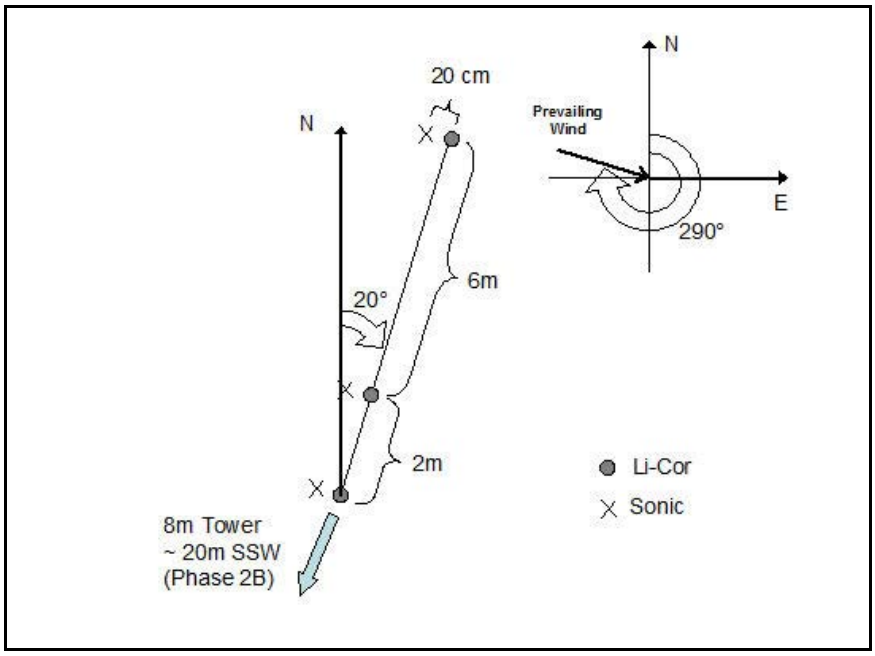

Figure 6. Horizontal array layout for Phase 2B (asymmetric placement).

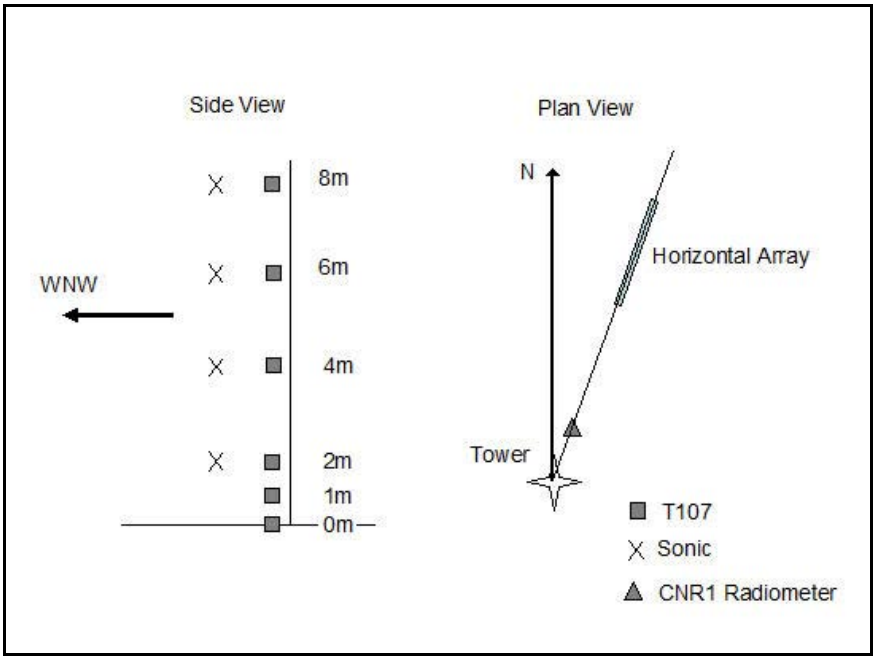

Figure 7. Tower layout for Phases 2A and 2B. Side and plan views of tower and surroundings are shown.

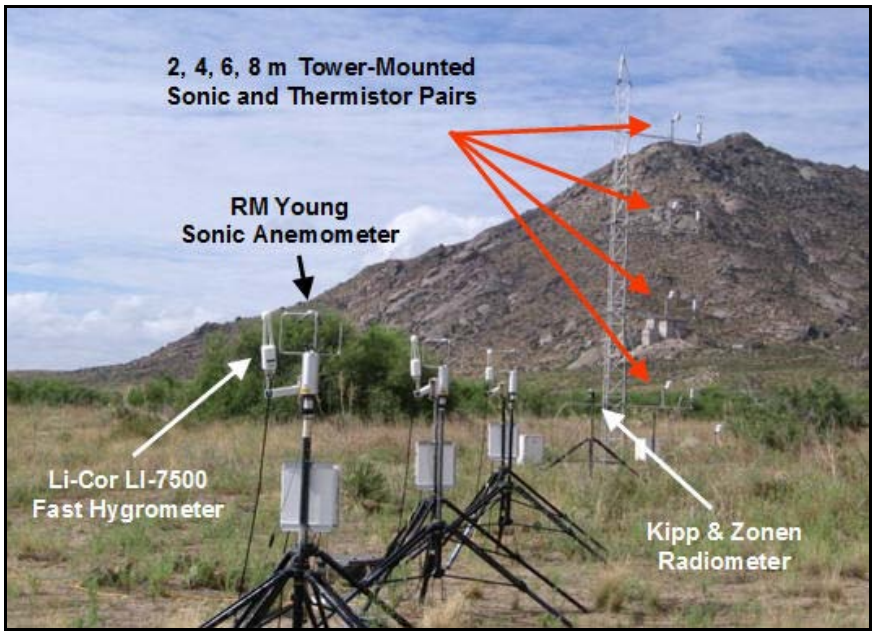

Figure 8. Photograph of the Phase 2A setup, 31 July 2007, looking approximately south.

3. Data Collection and Reduction

3.1 Data Collection Hardware and Methodology

The high speed sensors that were used in this measurement series included three Li-Cor model LI-7500 hygrometer sensor systems and eight R. M. Young model 81000 ultrasonic anemometers (hereafter referred to as "sonics"). These instruments were set to sample at 20 hertz (Hz), to provide high resolution data for water vapor concentration, temperature, and wind component fluctuations. A lower sample rate of 1 Hz was used for the Kipp and Zonen Model CNR1 shortwave and longwave infrared (IR) upward and downward flux sensor and for six model T107 temperature probes (which were mounted in louvered radiation shields). These last devices were used to check the accuracy of (and to normalize) the high speed temperature data measured by the sonic probes.

Three laptop computers were used to log data streams from the horizontal array and tower array sensor groupings. One laptop was located in a protective outdoor enclosure beside the tower, and archived serial (RS-232) data directly from the sonic wind sensors. This laptop also archived serial data from a Campbell CR-5000 micrologger that was connected to the T107 temperature probes and the CNR1 radiative flux sensor. A second laptop (also in a protective enclosure) located next to the horizontal sensor array archived serial data from the three Li-Cor water vapor sensors and three sonics that populated this array. The two outdoor laptops were connected by Ethernet links to a central hub, which was located in the horizontal array enclosure. A third laptop was then networked to the two data acquisition machines and used to examine

data and download completed hourly data files. The data link was also used to support a Network Time Protocol (NTP) synchronization of the laptop system clocks.

3.2 Auditing Data Quality

We used various procedures to ensure that the collected data was free of pathologies, and could be used for a reasonable analysis of trends and phenomena. The sonic data records ended with an error flag field that allowed for some degree of rejection of bad data. This particular automated check was embedded in the reduction programs that we wrote in support of this effort. Another check is one that flags fixed-length data records that are either too short or too long.

Automated techniques could not be used (at least at this point) in cases where the sensor doesn't flag questionable records or if the environment itself is causing physically incorrect sensor outputs. An instance of this is rain-induced malfunctions of the Li-Cor sensor readings. As an example, figure 9 shows data collected during a rain event, illustrating the importance of vetting data through graphical means. This example was from the evening of 25 May 2007, when a cluster of thunderstorms developed in the WSMR/Las Cruces, NM, region.

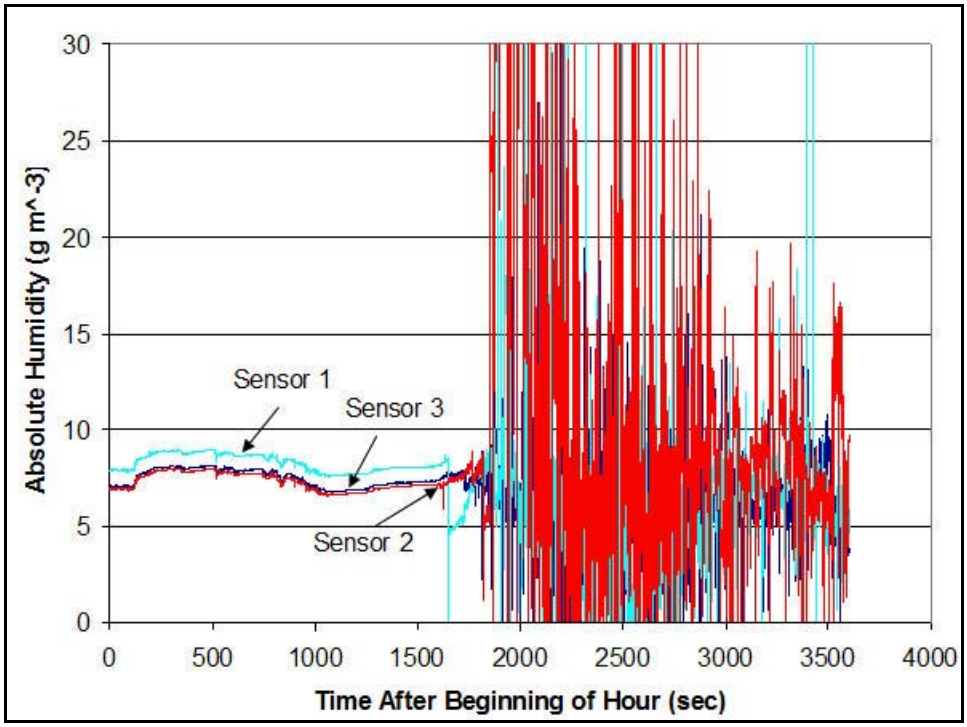

Figure 9. Li-Cor humidity sensor records for 25 May 2007, beginning at 2000 Mountain Daylight Time (MDT). Sensors were in a horizontal linear array, with a 2 m separation (Phase 1A configuration). Sensor 1 was the northernmost, sensor 3 was the southernmost.

Figure 10 shows the progress of the thunderstorm complex on local Doppler radar plots. The daily plot of water vapor concentration from one of the Li-Cor sensors appears normal until about 2030 MDT, when the range of fluctuations suddenly widens markedly. The plots in figure 10 indicate that the line of thunderstorms passed over the observation point sometime between

2000 and 2100 MDT, consistent with the timing of the hygrometer anomalies. The wild excursions of the humidity readings were probably caused by liquid rain water coating the windows of the transmissometer sensor. Although we set the Li-Cor Sensors up using the manufacturer's recommended tilt of the optical window relative to horizontal to permit rain water to shed, a persistent rain event appears to still seriously degrade accuracy until the windows are finally dry. It would perhaps be possible to provide a rain shield above the sensors, but that tactic would perturb the measurement results. It would also be possible that misting, wind driven rains and strong winds that frequently accompany thunderstorms could still easily erode the accuracy of the measurements or worse, damage the equipment setup.

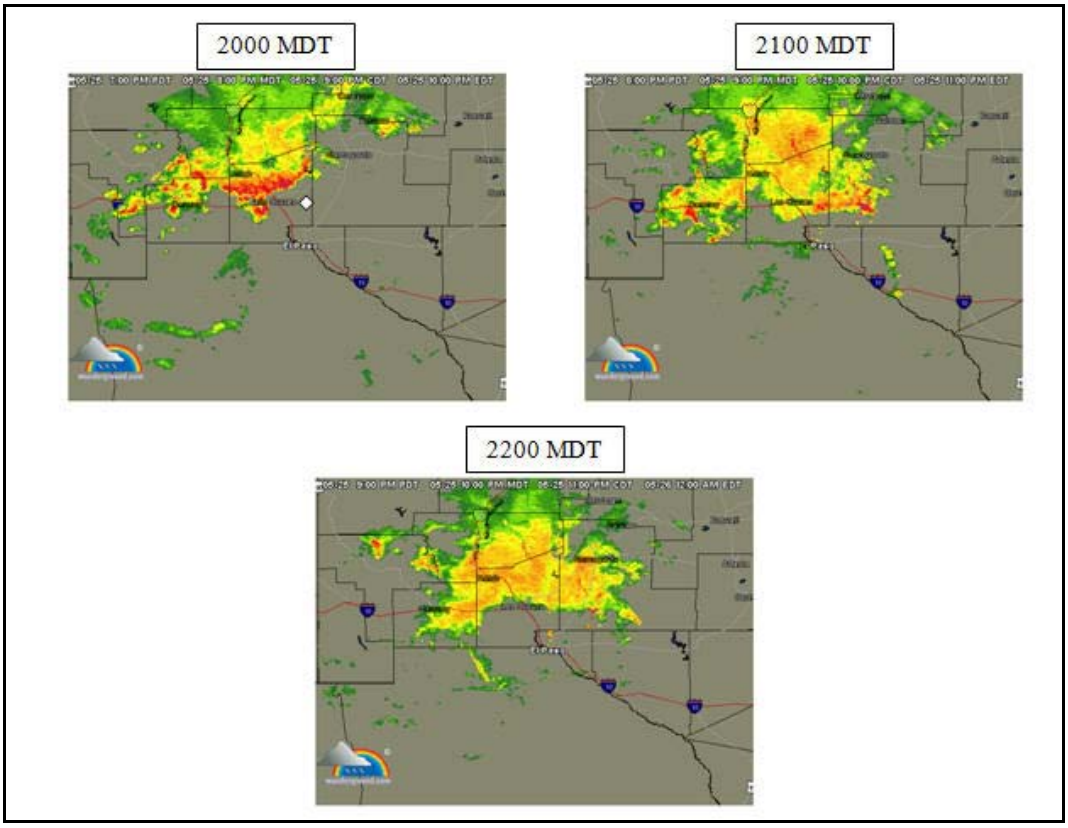

Figure 10. El Paso (EPZ) Doppler radar base reflectivity maps for 2000, 2100, and 2200 MDT, 25 May 2007. White diamond symbol on 2000 MDT plot depicts approximate location of observing site.

3.3 Daily Meteorological Summary Specifications

In our final data summary and analysis report, we will include archived daily summaries of conventional meteorological parameters observed for the WSMR, NM, region. These will include the following data, which will generally be presented in graphical form:

- Rawinsonde soundings for El Paso, TX, and WSMR, NM (when available)
- Air temperature

- Air pressure
- Dew point
- Wind speed
- Wind direction
- Surface weather summary (frontal position plots and synoptic discussion, when available)
- Precipitation radar (when rain events were seen in the area)
- Satellite: visible, IR, and water vapor imagery (when appropriate)

These parameters will serve to complement and check the temperature, pressure, wind component, and absolute humidity data that our high and low speed sensors collect in our test setup.

4. Data Analysis Products

4.1 Water Vapor Spatial Power Spectra

The water vapor molar density (milli-moles [mmol] m^{-3}) at each sampling point was converted to an absolute humidity (g m^{-3}) and a running mean was computed. The value of the absolute humidity fluctuation about this running mean was then computed at each sampling point. The high speed (20 Hz sampling rate) temporal data for the UVW wind velocity components were reduced to a spatial data set by computing 1 second sliding window averages of wind speed at each data point. This, multiplied by the sampling interval time, yielded a wind run position for the given point. Because the wind speed varied from point to point, the resulting spatial one-dimensional grid of data points was non-uniformly spaced. To better accommodate the analysis of the spectrum, which uses a fast Fourier transform (FFT) that expects uniformly-spaced points, the reduction software performed an interpolation of all of the points onto a uniform grid. The grid interval simply equals the total wind run divided by (N-1), where N is the total number of fluctuation data points.

The resulting regridded absolute humidity fluctuation data were windowed with a Hanning function and then transformed via an FFT; the power spectrum was then constructed from this result. Example spectra for Li-Cor sensor 1 data between 1700 and 1800 MDT on 25 May 2007, 1800–1900 MDT on 29 May 2007, and 0900–1000 MDT on 1 Aug 2007 are shown in figures 11–13. For the most part, this spectrum follows a Kolmogorov power law behavior (a straight line of –5/3 slope for log-log axes), although the spectral slope becomes significantly less negative at lower spatial frequencies (below about 0.1 m^{-1}). A sharp dip in the spectrum around 2×10^{-3} m^{-1} is apparent in figure 11 and to a lesser degree in the other plots. This dip is possibly

due to our selection of 500 m as the exponential weighting constant for computation of the running mean. At higher spatial frequencies (above about 1 m^{-1}), the spectral slope becomes more negative than the nominal –5/3 value. Another interesting difference between figure 11 and the other plots is the relatively high spectral power at the lowest spatial frequencies for the 25 May 2007 results. It is also evident that the point spectra shown here will not provide clear-cut estimates for the location of inner and outer scale humidity turbulence features. We will need to resort to cross-correlation and covariance methods to investigate departures from the inertial subrange and the structure of large scale humidity features.

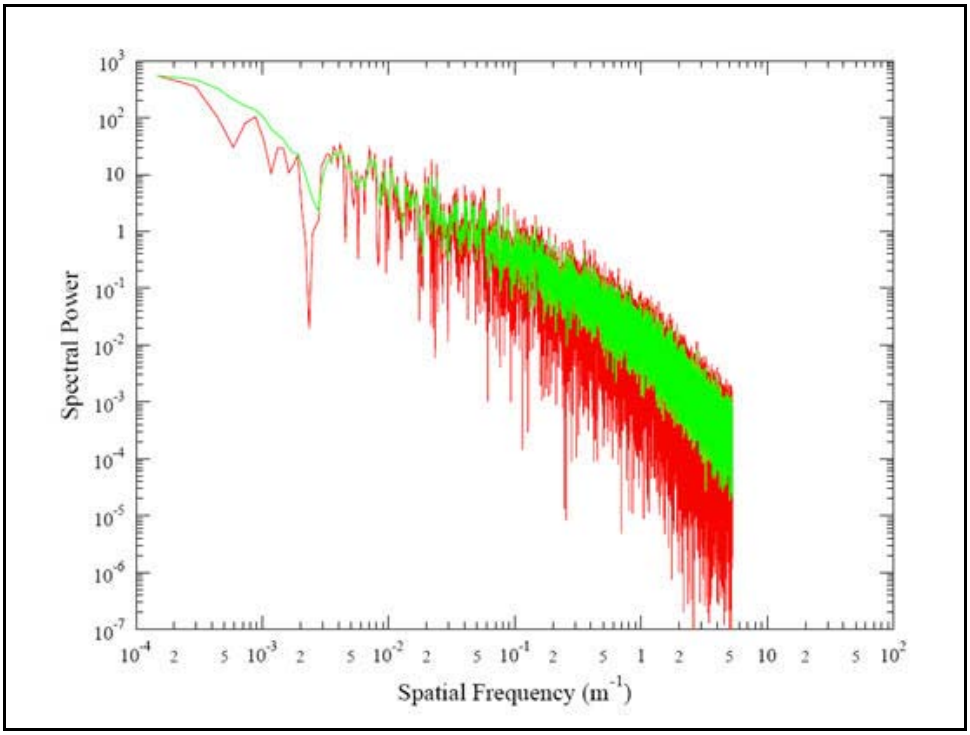

Figure 11. Example spatial power spectrum for 1700–1800 MDT on 25 May 2007. The red curve represents the full spectrum of about 72000 points, with the green curve representing a 5-point running mean.

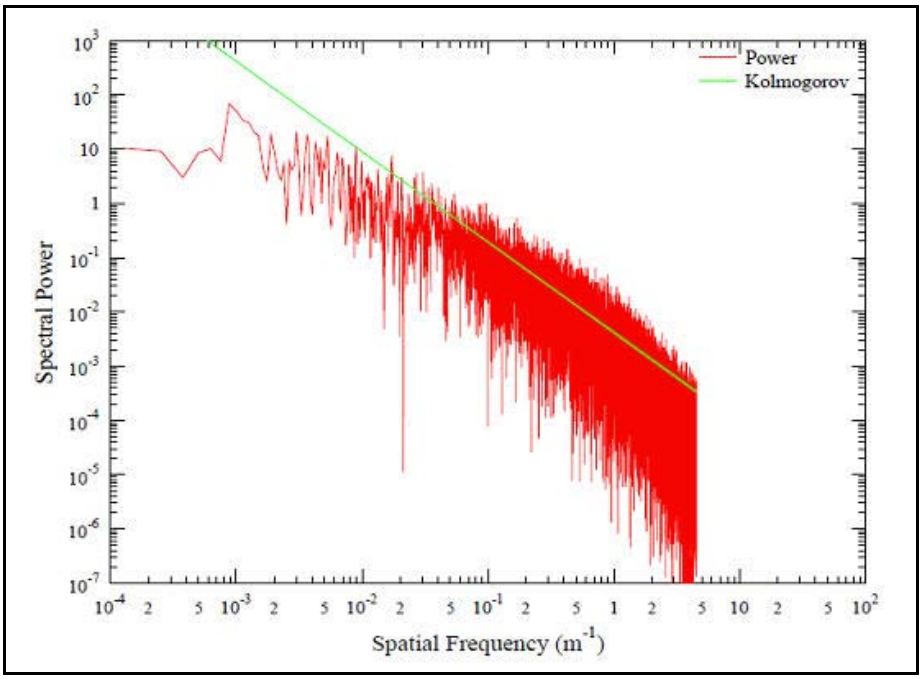

Figure 12. Spatial power spectrum for absolute humidity fluctuations for 1800–1900 MDT on 29 May 2007. Green line is –5/3 power law curve that intersects average near spatial frequency of 1 m^{-1}.

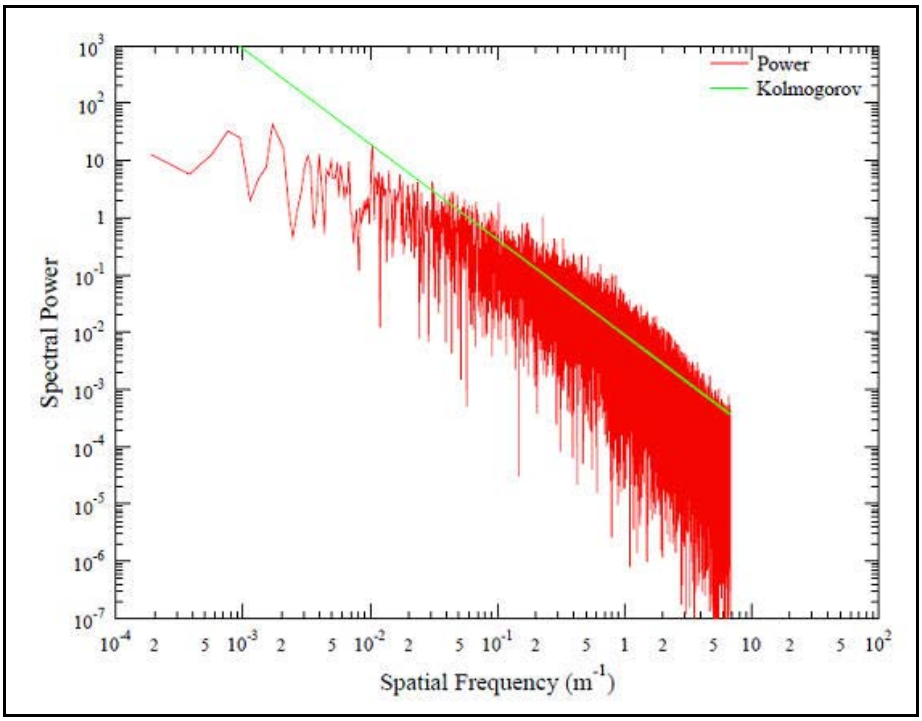

Figure 13. Spatial power spectrum for absolute humidity fluctuations for 0900–1000 MDT on 1 Aug 2007. Green line is –5/3 power law curve that intersects average near spatial frequency of 1 m^{-1}.

4.2 Cross-Correlation Temporal Results for Horizontal Array

One possible way to examine the existence and strength of large scale humidity fluctuations is through the calculation of the cross-correlation function between the absolute humidity ρ measured by sensors i and j:

$$\Gamma_{\rho}(t) = \int_{-\infty}^{\infty} \rho_i(t')\, \rho_j(t'+t)\, dt' \,. \tag{1}$$

This relation has to be numerically evaluated over the finite sampling domain by either direct numeric means or by application of the convolution theorem for Fourier transforms. We implemented both approaches and obtained good agreement in the results. The FFT approach will be used operationally, because it is much faster, and the data sets are extensive enough to warrant its use. Figure 14 shows the 25 May 2007 1500–1600 MDT results of the non-FFT calculation of cross-correlation between sensor sets 1–2, 2–3, and 1–3, which all have the same lag direction relative to the mean wind for the observing period. This consistent lag is reflected by the shift of the cross-correlation peak to negative values. The 1–3 correlation lag value (4 m baseline) is also roughly twice as large as the 1–2 or 2–3 values (2 m baseline), as expected. The maximum for the 1–3 correlation function is also lower than the 1–2 or 2–3 maxima, indicating the weaker intensity of larger humidity structures.

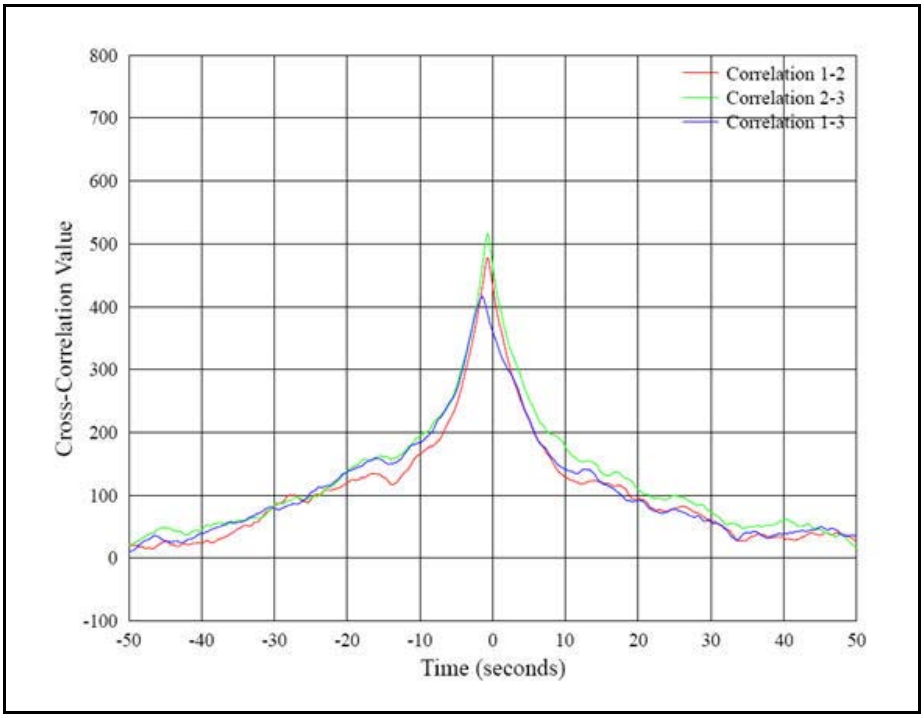

Figure 14. Example unnormalized cross-correlation for absolute humidity fluctuations for 1500–1600 MDT on 25 May 2007.

4.3 Heat and Momentum Fluxes

Other analysis products from the BLT experiment data are the sensible heat fluxes, latent heat fluxes and momentum fluxes that are derived from "instantaneous" fluctuations about running means for wind stream speed *u*, temperature *T*, vertical wind speed *w*, and absolute humidity ρ_w at time *t*:

$$u' = u(t) - < u >_t \ , \tag{2}$$

$$T' = T(t) - < T >_t \ , \tag{3}$$

$$w' = w(t) - < w >_t \ , \tag{4}$$

$$\rho'_w = \rho_w(t) - < \rho_w >_t \ , \tag{5}$$

where primes indicate the fluctuation value, and the running mean $<q>_t$ for quantity *q* is constructed using the iteration

$$< q >_t = (1 - e^{-\Delta t/\tau})\, q(t) + e^{-\Delta t/\tau} < q >_{t-\Delta t} \ , \tag{6}$$

where Δt is the time interval between data points (0.05 seconds in this case), and τ is the decay time constant for the running mean (60 seconds was used for this value in what follows). The vertical fluxes due to turbulent eddy transport are derived from standard developments (Stull, 1988):

$$H_S = \rho C_p < w'T' > \ , \tag{7}$$

$$\tau_m = \rho < u'w' > \ , \tag{8}$$

$$H_L = L_V < w'\rho'_w > \ , \tag{9}$$

where H_S is the sensible heat flux, τ_m is the momentum flux, H_L is the latent heat flux, ρ is the moist air density, C_p is the specific heat at constant pressure, and L_V is the latent heat of vaporization. A negative value of a quantity given by equations (7)–(9) indicates a net downward transport of that quantity. The sensible and latent heat fluxes given by equations (7) and (9) were computed for each wind-humidity sensor pair in the horizontal array. Typical 2 m AGL flux results for a relatively dry day (28 Jul 2007, preceded by a day with little precipitation) are shown in figure 15. Very little vertical moisture flux is apparent, but those fluctuations that do occur show mostly positive correlations with variations in the sensible heat flux during the daylight hours and negative correlations at night. With a few exceptions, the three sensor pairs also produce flux time series that correlate very well over periods down to 5-min scales. Figure 16 compares the sensor pair 3 flux results from figure 15 with the diurnal wind speed (in m sec^{-1}, divide by 20 to scale from plot axis) and absolute humidity (in g m^{-3}, divide by 10 to scale from axis) time series.

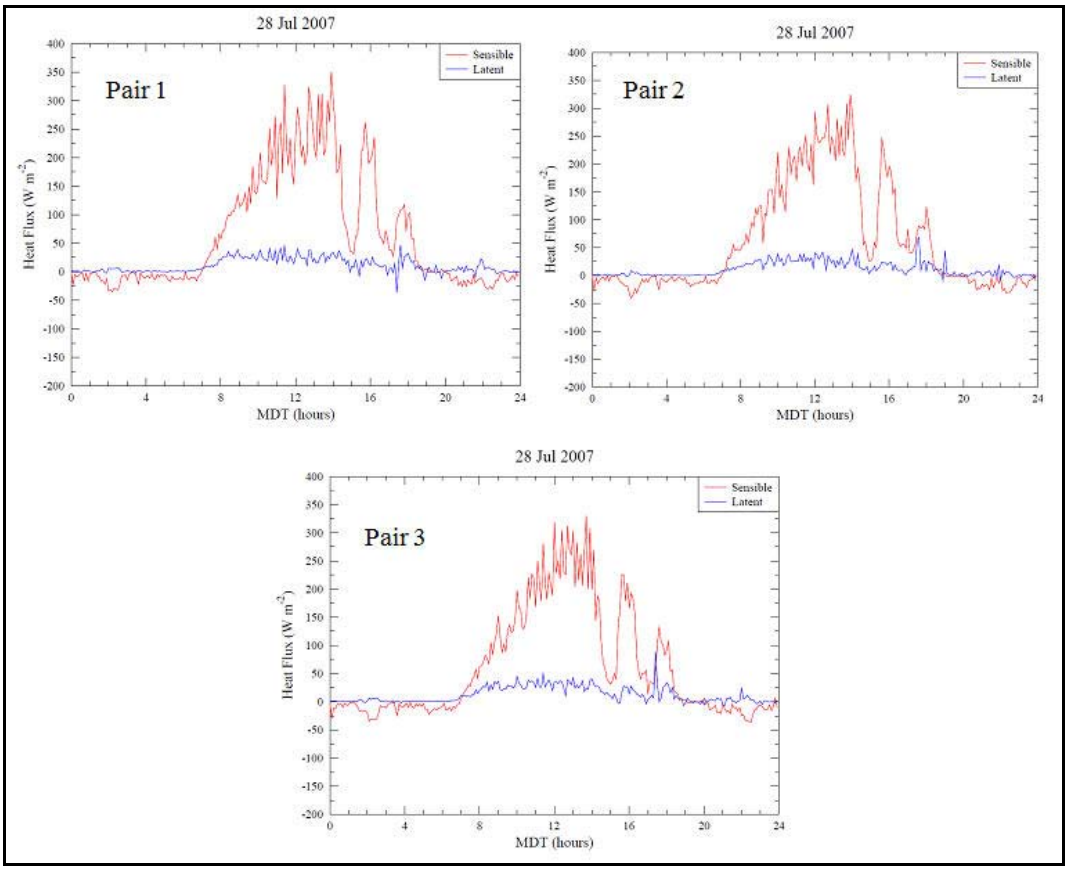

Figure 15. Comparison of diurnal variation of sensible and latent heat fluxes for the three sonic anemometer-hygrometer horizontal array sensor pairs for a typical dry day.

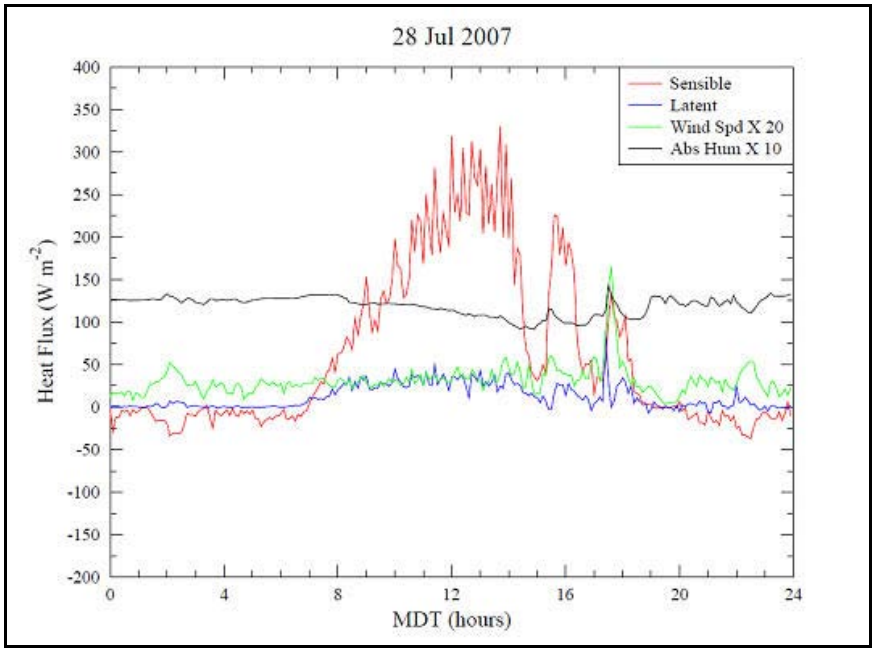

Figure 16. Comparison of sensible and latent heat flux time series with wind speed and absolute humidity for sensor pair 3 in the horizontal array.

There are two large afternoon dips in the sensible heat flux that are apparent on this plot which are likely due to cloud cover. At the trailing edge of the second sensible heat trough, between 1700 and 1800 MDT, there is a noticeable concurrent spike in wind speed, absolute humidity, and latent heat flux.

The cause of these concurrent spikes is probably due to downdraft gust outflow from a compact, fast-moving thunderstorm cell that passed just to the south of the observation site, moving from the northeast to the southwest. The base reflectivity radar archive maps for this date for 1700 and 1800 MDT are shown in figure 17.

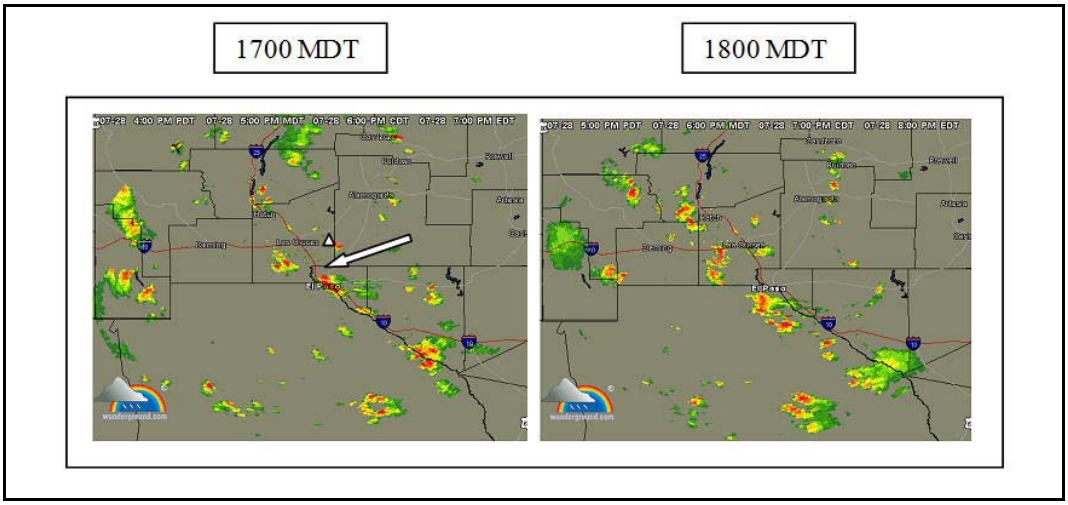

Figure 17. Radar base reflectivity maps for 28 Jul 2007 showing progress of compact storm cell near observation site. Approximate observation site location is indicated by white triangle on 1700 MDT plot, with approximate cell motion indicated by arrow.

Figure 18 compares the sensible and latent heat flux time series from a more moist day (28 May 2007) in the atypical year of 2007. The latent heat flux is much larger due to the moist soil that resulted from the unusually heavy rains in May. The daytime positive and nighttime negative correlations between the sensible and latent fluxes are more clearly seen than in the 28 Jul 2007 example shown above.

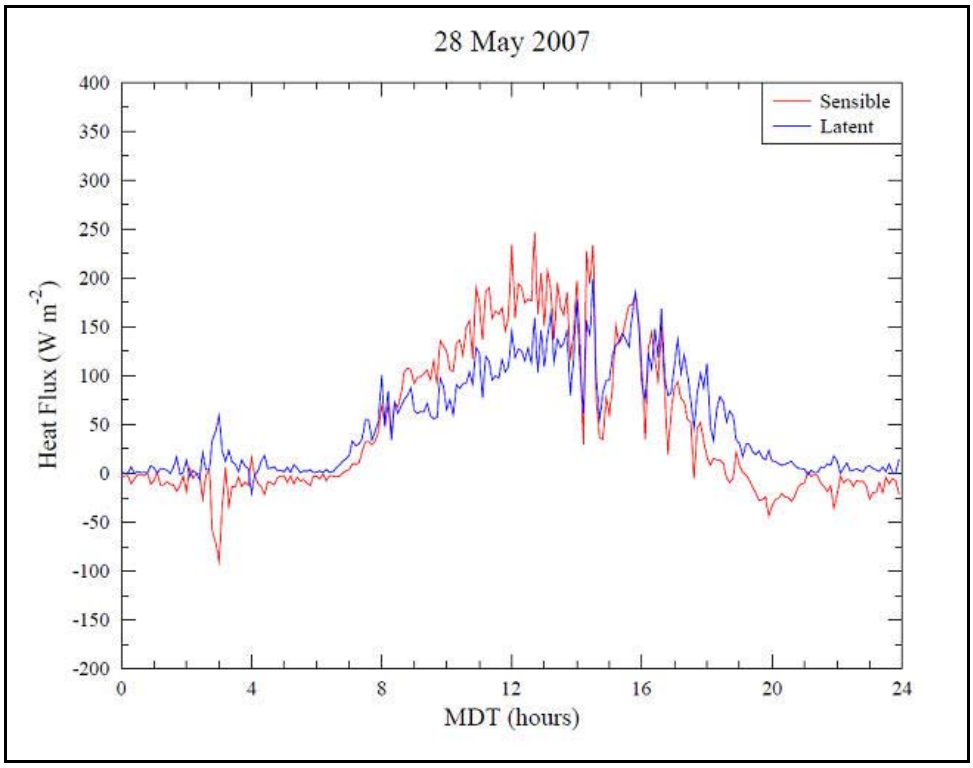

Figure 18. Comparison of sensible and latent heat fluxes for 28 May 2007.

Figure 19 depicts the evolution of an interesting anomaly that occurred during the night of 29–30 May 2007. The sensible heat flux went strongly negative (indicating unusually pronounced downward transport of thermal energy) after about 2000 MDT and stayed that way until shortly before 0400 the following morning. Sensor pair 1 was used to generate this panel of diurnal plots. Wind speed and absolute humidity are scaled as in figure 16. The source of this anomaly can be readily discerned by the behavior of the wind. The wind speed is seen to increase after 2100 MDT, creating a situation where heat is mixed down to the observation height of 2 m AGL. The wind speed begins to decrease after midnight and the sensible heat flux restores to a near zero value in the predawn hours. The absolute humidity varies over only a narrow range over this nighttime period, and the near-zero latent heat flux reflects this behavior.

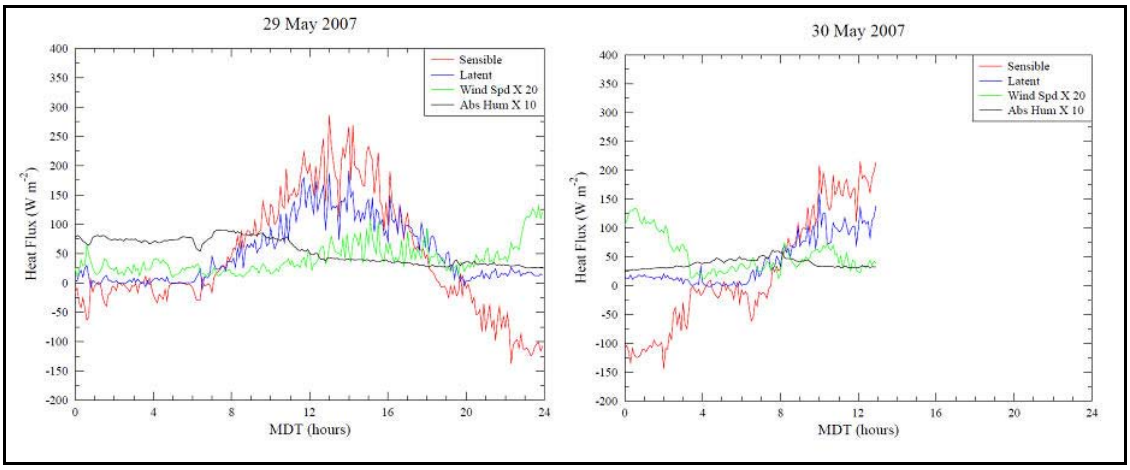

Figure 19. Sensible heat flux event during the night of 29–30 May 2007.

5. Discussion

These initial results indicate that many interesting daytime and nighttime boundary layer phenomena will be uncovered as we perform additional detailed spectral, cross correlation, and covariance analyses. Data auditing software has been developed to uncover problems with instruments and atmospheric conditions that might complicate or invalidate results from analysis software further down the reduction chain. We will continue to refine our reduction and analysis software to capture the temporal and spatial scales that can be observed for humidity fluctuations, and compare these with what might be expected from theory.

The advantage of having a measurement site that is easily secured, maintained and run on a continuous basis has been translated into a very useful database. The data sets span large periods of time and, because the sensors were allowed to collect data without interruption, a very valuable climatological reference data set for a desert environment will be available for future analysis. The availability of this resource is not a trivial consideration, because future deployments of THz or mid-wave infrared (MWIR) systems in desert environments are fairly likely. As our analysis proceeds, phenomena will probably be identified that will merit reconfiguration of the sensor layouts and combinations. These factors will be the subject of future discussion in subsequent analysis documents and open literature publications.

6. References

Deardorff, J. W. Efficient Prediction of Ground Surface Temperature and Moisture, With Inclusion of a Layer of Vegetation. *J. Geophys. Res.* **1978**, 83, 1889–1903.

O'Brien, S. G.; Tofsted, D. H. Development of a Terahertz Short Range Imaging Model, *Proceeding of the SPIE Defense and Security Conference*, Vol. 6239. Orlando, FL, 2006.

O'Brien, S. G.; Tofsted, D. H. Terahertz Target Fluctuation Estimates Derived from Field Measurements of Atmospheric Water Vapor, *Proceeding of the SPIE Defense and Security Conference*, Vol. 6949. Orlando, FL, 2008.

O'Brien, S. G.; Tofsted, D. H.; Yarbrough, J.; Scott Elliott, D.; Quintis, D. *Analysis of Boundary Layer Meteorological Data Collected at the White Sands Missile Range, International Test and Evaluation Association (ITEA) Modeling and Simulation Conference*, Las Cruces, NM, December 2007.

Oke, T. R. *Boundary Layer Climates*; Methuen & Co.: London, 1978.

Stull, R. B. *An Introduction to Boundary Layer Meteorology*; Kluwer Academic Publishers: Dordrect, The Netherlands, 1988.

List of Symbols, Abbreviations, and Acronyms

3D	three-dimensional
AGL	above ground level
ARL	U.S. Army Research Laboratory
BLT	Boundary Layer Turbulence
DARPA	Defense Advanced Research Projects Agency
EPZ	El Paso Doppler radar site code
FFT	fast Fourier transform
h	hour
Hz	hertz
IR	infrared
LIDAR	Light Detection and Ranging
MDT	Mountain Daylight Time
mmol	milli-mole
MWIR	mid-wave infrared
NTP	Network Time Protocol
NVESD	U.S. Army Night Vision and Electronic Sensors Directorate
S	south
THz	terahertz
TIFT	Terahertz Imaging Focal-plane-array Technology
W	west
WSMR	White Sands Missile Range

No. of Copies	Organization
1 PDF	ADMNSTR DEFNS TECHL INFO CTR DTIC OCP 8725 JOHN J KINGMAN RD STE 0944 FT BELVOIR VA 22060-6218
3 HCs	US ARMY RSRCH LAB ATTN RDRL CIM P TECHL PUB ATTN RDRL CIM L TECHL LIB ATTN IMNE ALC HRR MAIL & RECORDS MGMT 2800 POWDER MILL ROAD ADELPHI MD 20783-1197
1 CD	US ARMY RSRCH LAB ATTN RDRL CIM G TECHL LIB T LANDFRIED APG MD 21005-5066
1 CD	US ARMY RSRCH LAB ATTN RDRL ROE N W BACH PO BOX 12211 RESEARCH TRIANGLE PARK NC 27009
2 CDs	US ARMY RSRCH LAB ATTN RDRL CIE D S O'BRIEN WSMR NM 88002-5501
1 CD	US ARMY RSRCH LAB ATTN RDRL CIE M R SHIRKEY WSMR NM 88002-5501
1 CD	US ARMY RSRCH LAB ATTN RDRL CIE D D W HOOCK WSMR NM 88002-5501
1 CD	ARMY MATERIEL SYSTEMS ANALYSIS ACTIVITY ATTN AMXSY SC J MAZZ 392 HOPKINS ROAD APG MD 21005-5071
1 CD	US ARMY NIGHT VISION & ELECTRONIC SENSORS DIRECTORATE MEASUREMENT AND MODELING SERVICES BRANCH ATTN AMSRD CER NV MS MMS J HIXSON 0221 BURBECK ROAD FT BELVOIR VA 22060-5806
1 CD	ARMY MODELING & SIMULATION OFFICE DA G37 DAMO SBM 400 ARMY PENTAGON WASHINGTON DC 20310-0450
2 CDs	US ARMY RSRCH LAB ATTN RDRL CIE D D TOFSTED WSMR NM 88002-5501
1 CD	DIRECTOR USA TRADOC ANALYSIS CENTER ATTN ATRC W P BLECHINGER WSMR NM 88002-5502
1 CD	DIRECTOR USA TRADOC ANALYSIS CENTER ATTN ATRC WA L SOUTHARD WSMR NM 88002-5502
1 CD	ERDC/CRREL ATTN G KOENIG 72 LYME RD HANOVER NH 03755
1 CD	ARMY CORPS OF ENGINEERS TOPOGRAPHIC EENGINEERING CENTER DATA AND SIGNATURE ANALYSIS BRANCH FT BELVOIR VA 22060
1 CD	US MILITARY ACADEMY DEPT OF MATHEMATICAL SCIENCES THAYER HALL WEST POINT NY 10996-1786

No. of Copies	Organization
2 CDs	US MILITARY ACADEMY COMBAT SIMULATION LAB P WEST WEST POINT NY 10996
1 CD	AFRL IFOIL 525 BROOKS ROAD ROME NY 13441-4505
1 CD	AIR WEATHER SERVICE TECH LIBRARY FL4414 3 SCOTT AFB IL 62225-5458
1 CD	HQ USAFA/DFLIB 2354 FAIRCHILD DRIVE SUITE 3A10 USAF ACADEMY CO 80840-6214
1 CD	TECH CONNECT AFRL XPTC BLDG 16 RM 107 2275 D STREET WPAFB OH 45433-7226
1 CD	NAVAL RESEARCH LABORATORY A GOROCH MARINE METEOROLOGY DIVISION CODE 7543 7 GRACE HOPPER AVE MONTEREY CA 93943-5006
1 CD	US NAVAL WAR COLLEGE WAR GAMING DEPARTMENT CODE 33 686 CUSHING ROAD NEWPORT RI 2841-1207
1 CD	NAVAL POSTGRADUATE SCHOOL J D EAGLE OR ER 1 UNIVERSITY CIRCLE MONTEREY CA 93943
1 CD	NAVAL POSTGRADUATE SCHOOL R K WOOD OR WD 1 UNIVERSITY CIRCLE MONTEREY CA 93943
1 CD	NAVAL POSTGRADUATE SCHOOL G SCHACHER DEPT OF PHYSICS 1 UNIVERSITY CIRCLE MONTEREY CA 93943
1 CD	NAVAL POSTGRADUATE SCHOOL W B MAIER II DEPT OF PHYSICS 1 UNIVERSITY CIRCLE MONTEREY CA 93943
1 CD	RUTH H HOOKER RESEARCH LIBRARY 4555 OVERLOOK AVE SW WASHINGTON DC 20375
1 CD	NORTHROP GRUMMAN INFORMATION TECHNOLOGY M GOUVEIA 100 BRICKSTONE SQUARE ANDOVER MA 01810
1 CD	ANTEON CORP M ADAMS 46 GROWING RD HUDSON NH 03051
1 CD	SAIC ATTN MR DELGADO 731 LAKEPOINTE CENTRE DR O'FALLON IL 62269-3064
1 CD	TECHNICAL REPORTS BOULDER LABORATORIES LIBRARY MC 5 325 BROADWAY BOULDER CO 80305
1 CD	NCAR LIBRARY SERIALS NATIONAL CENTER FOR ATMOSPHERIC RESEARCH PO BOX 3000 BOULDER CO 80307-3000
1 CD	US ARMY NIGHT VISION & ELECTRONIC SENSORS DIRECTORATE SENSOR PERFORMANCE BRANCH ATTN AMSRD CER NV MS SP J REYNOLDS 10221 BURBECK ROAD FORT BELVOIR VA 22060-5806

No. of Copies	Organization
1 CD	US ARMY NIGHT VISION & ELECTRONIC SENSORS DIRECTORATE SENSOR PERFORMANCE BRANCH ATTN AMSRD CER NV MS SP R ESPINOLA 10221 BURBECK ROAD FT BELVOIR VA 22060-5806
1 CD	US ARMY NIGHT VISION & ELECTRONIC SENSORS DIRECTORATE SENSOR PERFORMANCE BRANCH ATTN AMSRD CER NV MS SP M FRIEDMAN 10221 BURBECK ROAD FT BELVOIR VA 22060-5806
1 CD	R RASMUSSEN NATIONAL CENTER FOR ATMOSPHERIC RESEARCH P O BOX 3000 BOULDER CO 80307-3000
1 CD	E JACOBS THE UNIVERSITY OF MEMPHIS DEPARTMENT OF ELECTRICAL AND COMPUTER ENGINEERING 206 ENGINEERING SCIENCE BLDG MEMPHIS TN 38152-3180

Total: 43 (1 PDF, 3 HCs, 39 CDs)